10,08,13

Dependences of the specific surface energy on the size and shape of the nanocrystal under various $P-T$ conditions

© M.N. Magomedov

Institute for geothermal problems and renewable energy —
branch of the joint Institute of high temperatures of the Russian Academy of Sciences,
Makhachkala, Russia

E-mail: mahmag4@mail.ru

Received December 21, 2023
Revised January 8, 2024
Accepted January 17, 2024

Based on the RP model, the dependences of the specific surface energy σ and surface pressure P_{sf} on the size (N) and shape of the nanocrystal at different values of pressure P and temperature T are studied. Calculations for a gold nanocrystal have shown that at $P = 0$, the $P_{sf}(N)$ function lies in the negative region, i.e. the nanocrystal is stretched by surface pressure the more the temperature is higher, or the more the nanocrystal shape deviates from the most energy-optimal shape. With a decrease in N value at $P = 0$, the $\sigma(N)$ function decreases the more noticeably the higher the temperature, or the more the nanocrystal shape deviates from the most energy-optimal shape. Based on these results, it is shown that obtained in some articles the increase in the $\sigma(N)$ function with an isomorphically-isothermal decrease in N does not correspond to the physical properties of the nanocrystal. In these articles, the nanocrystal was compressed by surface pressure, which increased with an isomorphically-isothermal decrease in N value. This compression led to a corresponding increase in the $\sigma(N)$ function both with an isomorphic-isothermal decrease in size and with an isomeric (i.e., at $N = \text{const}$) increase in the temperature of the nanocrystal.

Keywords: Gibbs surface, Tolman length, surface pressure, equation of state, gold.

DOI: 10.61011/PSS.2024.03.57947.272

1. Introduction

The specific (per unit area) surface energy (σ) of a macrocrystal is one of key parameters that govern its strength and adhesion properties. Therefore, considerable attention is being paid to the determination of σ values. However, experimental measurements of σ in the solid phase are remarkably laborious and are feasible only at high temperatures [1,2]. Notably, even at high temperatures, the accuracy of σ measurement is very low. This is the reason why much attention is being paid to theoretical predictive modeling of σ for macrocrystals.

Various properties of nanocrystals have been examined over the last few years, and a considerable number of theoretical studies focused on the dependence of σ on the nanocrystal size have been published within this context. This issue is made topical by the fact that the dependence of σ on the size or the number of atoms (N) of a nanocrystal governs the size dependences of all nanocrystal lattice properties. Unfortunately, an experimental $\sigma(N)$ dependence has not been reported yet, since the surface properties of a nanocrystal are hard to measure. In view of this, numerous studies focused on the methods for calculation of function $\sigma(N)$ have still not provided a conclusive answer to the question of whether function $\sigma(N)$ decreases or increases with an isomorphic (i.e., with the nanocrystal shape being fixed) reduction in the number of atoms (N) in a nanocrystal under constant pressure P and temperature T levels. Theoretical papers arguing both for a decrease (this is reported primarily in analytical studies) and an increase (this was determined via computer modeling) of σ with an isomorphic reduction in size of a nanoparticle (either solid or liquid) have been published in recent times (see reviews in [3–7]).

For example, a combination of atomistic modelling and continuum mechanics was used to study a spherical core–shell model with radius r in recent paper [5]. The results of calculations performed in [5] for a gold nanocrystal at $T = 0\,\text{K}$ revealed that function $\sigma(r)$ increases with an isomorphic reduction in radius of a nanocrystal. The authors of [6] have examined the variation of function σ with isomorphic changes in the size and temperature of metallic nanoparticles in both solid and liquid states. Interatomic potentials of N bodies and the Monte Carlo method were used in [6]; in addition, analytical calculations were performed. A solid nanocrystal and a liquid nanodroplet were examined at temperatures $T = 5\,\text{K}$ and $T = 1500\,\text{K}$, respectively. It was found in [6] that σ for a nanoparticle with a free surface increases with an isomorphic-isothermal reduction in the size of a nanoparticle in both solid (σ_s) and liquid (σ_l) phases.

The authors of studies reporting an increase of σ with an isomorphic-isothermal reduction in the nanoparticle size take advantage of the fact that no experimental dependence of σ on the nanoparticle size has been published in

literature. This allows them to claim that the obtained results are accurate. However, although an experimental $\sigma(N)$ dependence has not been reported, function $\sigma(N)$ has a certain physical meaning and is related to other characteristics of a nanoparticle that could be measured (e.g., melting point). Therefore, the results of studies supporting an increase of σ with an isomorphic-isothermal reduction in the nanoparticle size are incompatible with the physical characteristics of actual metallic nanoparticles for the following reasons.

1. It has been accepted since the times of Tolman that σ_{l} decreases with a reduction in the size of a nanodroplet [8]. According to Tolman, the dependence of σ_{l} on radius r of a spherical nanodroplet of a single-component liquid may be presented in the following form [8,9]:

$$\sigma_{\text{l}}(r) = \frac{\sigma_{\text{l}}(\infty)}{1 + 2\frac{\delta}{r}} \cong \sigma_{\text{l}}(\infty)\left(1 - 2\frac{\delta}{r}\right).$$

Here, $\sigma_{\text{l}}(\infty)$ is the surface energy of a macrodroplet and $\delta = r_e - r$ is the difference between the equimolar radius and the nanodroplet radius; δ is also called the Tolman length.

Different expressions have been proposed for the calculation of δ. For example, the following relations were obtained for relatively large droplets:

$$\delta = d_a \text{ [10]},\ 0.725d_a \text{ [11]},\ r_{\text{o}}/3 \text{ [12]},\ 0.376r_{\text{o}} \text{ [13]},$$

where d_a is the atom diameter and r_{o} is the coordinate of the minimum of the 6–12 Mie–Lennard-Jones interatomic potential. In addition, it was found in [9] that $\delta = \alpha_{\text{m}}/4$, where α_{m} is a parameter characterizing the size dependence of melting point T_{m} for a spherical nanocrystal under atmospheric pressure ($P = 1$ atm):

$$T_{\text{m}}(r) = T_{\text{m}}(\infty)\left(1 - \frac{\alpha_{\text{m}}}{2r}\right) = T_{\text{m}}(\infty)\left(1 - \frac{2\delta}{r}\right).$$

The values of δ for 49 solid metals were calculated in [9], and δ values for liquid inert gases were calculated in [13]. All these data demonstrate that $\delta > 0$. This contradicts the dependences obtained in studies where σ increases with an isomorphic-isothermal reduction in the nanoparticle size.

2. It was demonstrated in [6, Figure 2] that the value of σ_{s} increases by a factor of almost 2 (from 1.1–1.2 to 1.9–2 J/m^2) as the radius of a copper (Cu) crystal decreases from a macroscopic level ($r = \infty$) to $r = 5$ Å. The experimental specific surface energy value for a Cu macrocrystal is $\sigma_{\text{s}}(\infty) = 2 \pm 0.1$ J/m^2 [14]. However, if we assume that the mentioned result from [6, Figure 2] is correct (i.e., $\sigma_{\text{s}}(r = 5\,\text{Å})/\sigma_{\text{s}}(r = \infty) = 2/1.2 = 1.67$), a copper nanoparticle with a radius of 5 Å should have specific surface energy

$$\sigma_{\text{s}}(r = \infty) = 1.67 \cdot (2 \pm 0.1)\,\text{J/m}^2 = 3.34 \pm 0.167\,\text{J/m}^2.$$

According to [14], the experimental values of $\sigma_{\text{s}}(\infty)$ for molybdenum (Mo) and tungsten (W) macrocrystals are 2.91–3.00 J/m^2 and 3.265–3.68 J/m^2, respectively. Thus, according to [6], the value of σ for a Cu nanocrystal with radius $r = 5$ Å should reach a level corresponding to the specific surface energies of Mo or W macrocrystals [14].

3. It was found in the study of a Cu nanodroplet (see [6, Figure 7]) that σ_{l} increases from $\sigma_{\text{l}}(r = \infty) = 1.2$ J/m^2 to $\sigma_{\text{l}}(r = 5\,\text{Å}) = 2.3$ J/m^2. This is also a surprising result, since the following relation between the surface energies of solid and liquid phases was determined experimentally for macrosystems: $\sigma_{\text{s}}/\sigma_{\text{l}} = 1.09$–$1.33$ [1,15]. At the same time, it was demonstrated in [16] that ratio $\sigma_{\text{s}}/\sigma_{\text{l}}$ drops to unity as the number of atoms in a nanosystem decreases. Therefore, if σ_{l} reaches the values typical of a macrocrystal as a nanodroplet grows smaller, this nanodroplet should crystallize. Notably, the value of $\sigma_{\text{l}}(T = 1500\,\text{K})$ in [6, Figures 2 and 7] exceeds the value of $\sigma_{\text{s}}(T = 5\,\text{K})$ in both macro- and nanosystems. This result clearly contradicts the laws of nanoparticle physics.

4. As for experimental studies into the size dependence of the specific surface energy, such experiments for the liquid phase were performed in [17,18]. It was found that function $\sigma_{\text{l}}(r)$ decreases with nanodroplet size. One may also cite the results from [19], where a system of submillimeter grains acoustically levitated in air was studied. These levitating grains self-assemble into a monolayer of particles, forming mesoscopic granular rafts that behave as liquid droplets. It was found in [19] that the effective surface tension and the elastic modulus of a raft decrease with raft size.

All these inconsistencies cast doubt upon the correctness of techniques for calculation of the surface energy that were used in theoretical studies revealing an increase of σ with an isomorphic-isothermal reduction in the nanoparticle size. The following relevant questions then arise:

1. Why did the authors of [5,6] and other studies focused on computer modeling find that the value of σ increases with an isomorphic-isothermal reduction in the nanoparticle size?

2. How a correct dimensional dependence of function $\sigma(N)$ may be obtained?

3. How does this size $\sigma(N)$ dependence varies under different P–T conditions?

In the present study, these questions are answered within equilibrium and reversible thermodynamics. A proprietary analytical method for calculation of function $\sigma(T, P, N)$, which is called the RP model, is used for this purpose. For the first time, dependences of the specific surface energy and the surface pressure on the size of a nanocrystal and the shape of its surface were calculated within the RP model for gold and examined under different P–T conditions. The obtained results are used to pinpoint the errors of authors of those studies where an increase of function $\sigma(N)$ with an isomorphic-isothermal reduction in the nanocrystal size was reported.

2. Method for calculation of the surface properties of a nanocrystal

The basics of the RP model have been outlined in our study [20], and the results of its further development have been reported in [21–23]. It is assumed in this model that a nanocrystal has the shape of a rectangular parallelepiped with a square base. Its shape may be adjusted by varying shape parameter f.

Let us consider a condensed nanosystem of N identical atoms bounded by the Gibbs surface. The pair interatomic interaction is represented by the Mie–Lennard-Jones potential in the form

$$\phi(r) = \frac{D}{(b-a)}\left[a\left(\frac{r_o}{r}\right)^b - b\left(\frac{r_o}{r}\right)^a\right], \qquad (1)$$

where D and r_o are the depth and the coordinate of the potential minimum, $b > a > 1$ are numerical parameters, and r is the distance between atom centers.

With the „only nearest neighbors interaction" approximation applied, the following expressions were obtained in [21–23] within the RP model for the specific surface energy of face (100) of a nanocrystal and surface pressure P_{sf}:

$$\sigma(N, f) = -\frac{k_n(\infty)DR^2}{12\alpha^{2/3}r_o^2} L_E(N, f), \qquad (2)$$

$$P_{sf} = P_{Lp}(1-\Delta_p) = \frac{4\alpha^{1/3}Z_s(f)}{N^{1/3}c}\sigma(1-\Delta_p). \qquad (3)$$

Here, $R = r_o/c$ is the relative linear density of a crystal, $c = (6k_p v/\pi)^{1/3}$ is the average (over the nanosystem volume) distance between the centers of neighboring atoms, k_p is the packing coefficient of a structure consisting of N atoms, $k_n(\infty) = k_n(N=\infty)$ is the coordination number for a macrocrystal, $\alpha = \pi/(6k_p)$ is the structure parameter, and $f = N_{ps}/N_{po}$ is the shape parameter of a rectangular parallelepiped that is specified by the ratio of number N_{ps} of atoms at its side edge to number N_{po} of atoms at the edge of the square base. Laplace pressure P_{Lp} and the functions introduced in (2) and (3) are written as

$$P_{Lp} = \frac{4\alpha^{1/3}Z_s(f)}{N^{1/3}c}\sigma = 4\frac{(1-k_n^*)}{\alpha^{1/3}c}\sigma, \qquad (4)$$

$$Z_s(f) = \frac{1+2f}{3f^{2/3}},\ L_E(N, f) = U(R) + 3H_w(N, T),$$

$$\Delta_p = -\frac{1}{2}\left[\frac{\partial \ln(\sigma)}{\partial \ln(c)}\right]_{T,N,k_p,f} = 1 + \frac{1}{2L_E(N, f)} \times \left\{U'(R) - 9\left[q - \gamma t_y\left(\frac{\Theta_E}{T}\right)\right]H_w(N, T)\right\}, \qquad (5)$$

$$H_w(N, T) = \frac{6\gamma(N, f)k_n(\infty)}{(b+2)}\left[\frac{k_B\Theta_E(N, f)}{Dk_n^*}\right]E_w\left(\frac{\Theta_E}{T}\right), \qquad (6)$$

$$k_n^* = \frac{k_n(N, f)}{k_n(\infty)} = 1 - Z_s(f)\left(\frac{\alpha^2}{N}\right)^{1/3}, \qquad (7)$$

$$U(R) = \frac{aR^b - bR^a}{b-a},$$

$$U'(R) = R\left[\frac{\partial U(R)}{\partial R}\right] = \frac{ab(R^b - R^a)}{b-a},$$

$$E_w(y) = 0.5 + \frac{1}{[\exp(y)-1]},\ t_y(y) = 1 - \frac{2y\exp(y)}{[\exp(2y)-1]}.$$

Here, $k_n(N, f)$ is the average (over the entire nanosystem) value of the first coordination number, k_B is the Boltzmann constant, Θ_E is the Einstein temperature, and $\gamma = -(\partial \ln\Theta_E/\partial \ln v)_T$, $q = (\partial \ln\gamma/\partial \ln v)_T$ are the first and the second Grüneisen parameters. The formulae for calculation of these functions were given in [21–23].

In the „thermodynamic limit" (i.e., when $N \to \infty$ and system volume $V \to \infty$ at $v = V/N = \text{const}$), expression (7) yields the following: $k_n^*(N \to \infty) \to 1$. Functions P_{Lp} in (4) and P_{sf} in (3) then vanish, and the expressions from (2), (5), and (6) transform into formulae for a macrocrystal.

The presented RP model provided an opportunity to examine the dependences of the specific surface energy both on the size (number of atoms N) and on the surface shape (f) of a nanocrystal at different temperatures and pressures (see [22–28]). The application of this method and the obtained results were discussed in detail in the indicated studies.

3. Calculation results for gold

Gold (Au, $m(\text{Au}) = 196.967$ a.m.u.) was chosen for calculations of the dependence of the surface energy on the nanocrystal size. Gold has a face-centered cubic (FCC) structure ($k_n = 12$, $k_p = 0.7405$, $\alpha = \pi/(6k_p) = 0.70709$) and does not undergo any polymorphic phase transitions up to 220 GPa [29].

The parameters of pair interatomic potential (1) for FCC Au were determined with the use of a self-consistent method in our study [23]. They have the following values:

$$r_o = 2.87 \cdot 10^{-10}\,\text{m},\ D/k_B = 7446.04\,\text{K},$$

$$b = 15.75,\ a = 2.79. \qquad (8)$$

As was demonstrated in our studies [24,30,31], potential (1) with parameters from (8) provides a fine agreement with experimental data for all thermodynamic properties and the baric dependence of the melting point of a macrocrystal of FCC Au. Therefore, in the present study, variations of the equation of state and the surface energy in transition from a macrocrystal to a nanocrystal were examined with the use of potential (1) with parameters from (8).

Calculations were performed for a nanocrystal of $N = 306$ atoms with a free geometric Gibbs surface. This specific number of atoms was chosen for the following reasons. On the one hand, we tried to illustrate most vividly the difference in baric dependences for macro- and

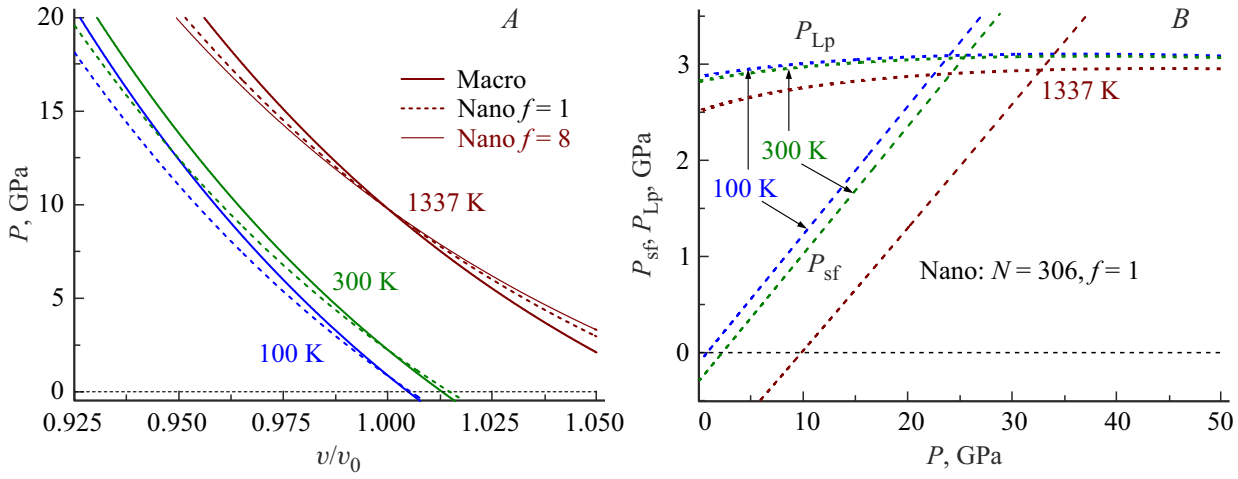

Figure 1. *A* — Isomorphic-isomeric dependences of pressure on normalized volume for FCC Au. Thick solid curves and dashed curves correspond to a macrocrystal and a cubic nanocrystal, respectively. The thin solid curve for 1337 K represents the result for a rod-shaped nanocrystal. From bottom to top, the following isotherms are shown: $T = 100$, 300, and 1337 K. *B* — Isomorphic-isomeric baric dependences of Laplace pressure P_{Lp} and surface pressure P_{sf} for a cubic nanocrystal consisting of 306 atoms. From top to bottom, the following isotherms are shown: $T = 100$, 300, and 1337 K.

nanosized systems. On the other hand, as was noted in [16,32–35], the difference between liquid and solid phases vanishes at a certain number of atoms (N_0). Thus, the thermodynamic concept of a liquid or solid phase is no longer applicable to a cluster at $N \leq N_0$. It was determined theoretically for metals at $P = 0$ that

$$N_0 = 50{-}300 \text{ [16,32,34]}.$$

The value of $N = 306$ was also chosen for the purpose of examining the effect of nanocrystal shape on the size dependence of surface properties. The bulk of calculations were carried out for a nanocrystal of $N = fN_{po}^3/\alpha = 306$ atoms having the energetically optimum shape of a rectangular parallelepiped (i.e., the shape of a cube): $f = 1$, $N_{po} = 6$, $k_n^* = 0.882152$, $k_n = 10.5858$. However, calculations were also performed for a nanocrystal of $N = fN_{po}^3/\alpha = 306$ atoms shaped like a rod (i.e., at $f = 8$, $N_{po} = 3$, $N_{ps} = N_{po}f = 24$, $k_n^* = 0.833048$, $k_n = 9.99658$). This provided an opportunity to examine the variation of properties with an isothermal-isobaric change in the nanocrystal shape.

Figure 1, *A* presents isomorphic-isomeric dependences (i.e., dependences at constant f and N values) of pressure (P, GPa) on normalized volume ($v/v_o = (c/r_o)^3 = R^{-3}$) for macro- and nanocrystals of FCC Au. Calculations were performed along three isotherms: 100, 300, and 1337 K. Solid and dotted curves correspond to a macrocrystal (i.e., $N = \infty$) and a cubic nanocrystal of $N = 306$ atoms, respectively. The thin solid curve for 1337 K represents the result for a rod-shaped nanocrystal. The magnitude of pressure rise in a nanocrystal is lower than the one in a macrocrystal, indicating a reduction in the elastic modulus ($B_T = -v(\partial P/\partial v)_T$) occurring as a nanocrystal grows smaller. A decrease of B_T with a reduction in the nanocrystal size has also been noted in theoretical and experimental studies performed by other research groups [36–40].

It can be seen from Fig 1, *A* that dependences $P(v/v_o)$ for nano- and macrocrystals intersect at a certain value of relative volume $(v/v_o)_0$. Thus, surface pressure $(P_{sf}(v) = P(v)_{Macro} - P(v)_{Nano})$ becomes zero at $(v/v_o)_0$: $P_{sf}(v/v_o)_0 = 0$. At $v/v_o < (v/v_o)_0$, the surface pressure compresses a nanocrystal ($P_{sf} > 0$); at $v/v_o > (v/v_o)_0$, a nanocrystal is stretched: $P_{sf} < 0$. The value of $(v/v_o)_0$ decreases under both an isomorphic-isomeric temperature rise T and an isomorphic-isothermal N reduction. It also follows from Figure 1, *A* that the pressure in a nanocrystal goes through zero at a v/v_o value that is higher than the one for a macrocrystal. It can be seen from Figure 1, *B* that the surface pressure rise with pressure is more pronounced than the corresponding Laplace pressure increase. While $P_{Lp} > P_{sf}$ is satisfied under low pressures, this inequality is reversed under high pressures.

Figure 2 shows the calculated baric (*A*) and temperature (*B*) isomorphic-isomeric dependences of the specific surface energy (σ, J/m^2 = N/m) for face (100) in FCC Au. Solid and dotted curves correspond to a macrocrystal and a cubic nanocrystal consisting of $N = 306$ atoms, respectively. Thin solid curves in Figures 2, *A* and *C* represent the 1337 K isotherm for a rod-shaped nanocrystal. As was demonstrated in [30], our calculations of the $\sigma(100)$ value for a macrocrystal of FCC Au agree well with the experimental and theoretical (in brackets) estimates made in other studies:

$$\sigma(100)/[\text{J/m}^2] = 1.54\ (T = 0\,\text{K}) - 1.333\ (T_m = 1337\,\text{K})\ [1],$$

$$(1.363\ (T = 0\,\text{K}))\ [4],\quad (1.359\ (T = 0\,\text{K}))\ [14].$$

It can be seen from Figure 2, *A* that at lower temperatures, a pressure region emerges where the specific surface

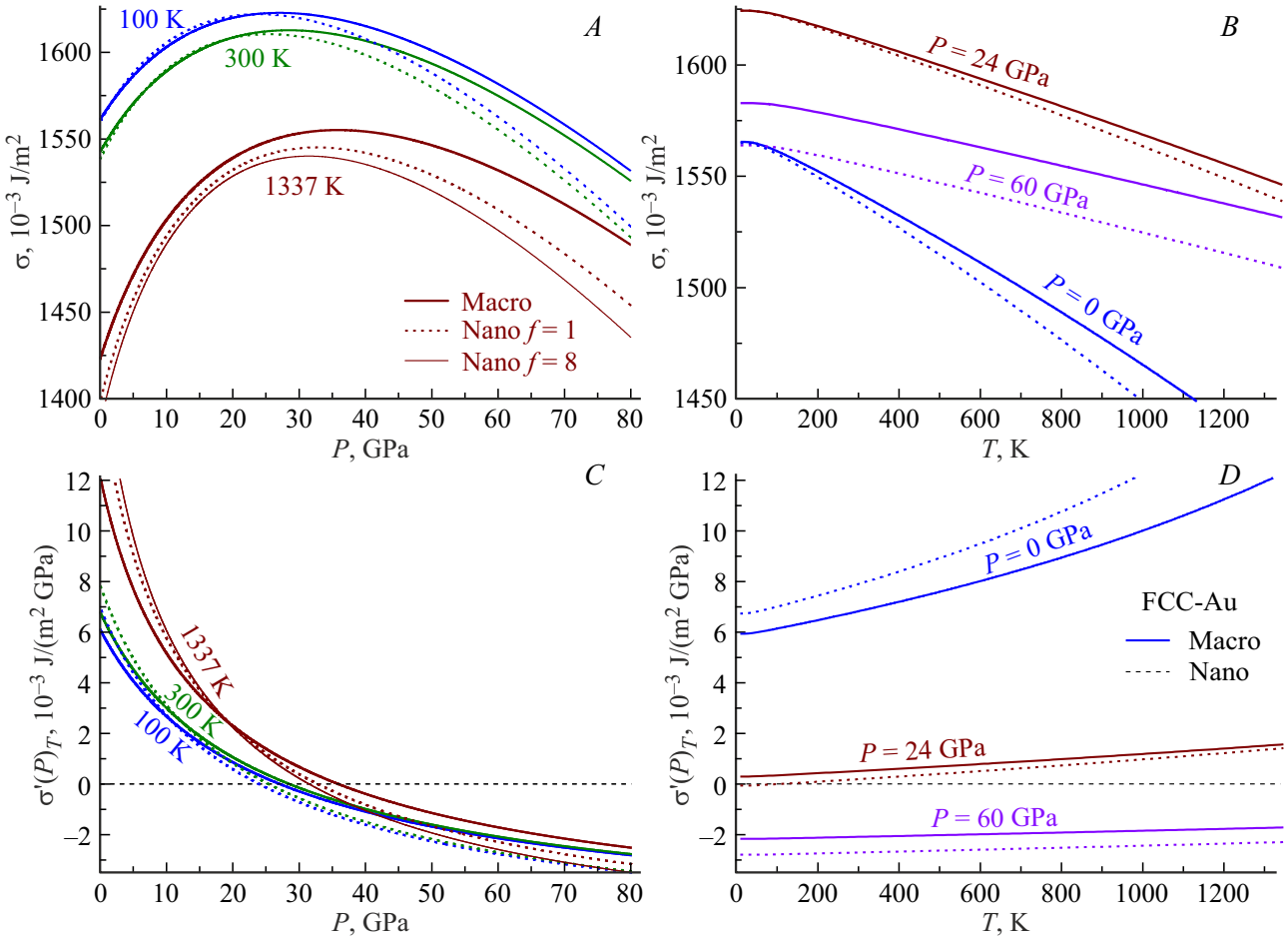

Figure 2. Baric (A) and temperature (B) isomorphic-isomeric dependences of specific surface energy $\sigma(100)$ are shown in the upper plots. The lower plots show baric (C) and temperature (D) isomorphic-isomeric dependences of the isothermal derivative of $\sigma(100)$ with respect to pressure: $\sigma'(P) = (\partial\sigma/\partial P)_T$. From top to bottom, the following isotherms are shown in the plots on the left: $T = 100$, 300, and 1337 K. The following isobars are shown in the plots on the right: $P = 0$, 24, and 60 GPa. Solid and dotted curves correspond to a macrocrystal and a cubic nanocrystal, respectively. Thin solid curves in Figures 2, A and C correspond to the 1337 K isotherm for a rod-shaped nanocrystal.

Surface properties of FCC Au

T, K	v/v_o	$\sigma(100)$, 10^{-3} J/m^2	Δ_P	P_{Nano}, GPa P_{Macro}, GPa	σ_{max}, 10^{-3} J/m^2	P_{max}, GPa
100	1.00487 1.00547	1561.19 1559.84	1.0299 1.0342	0.090 −0.101	1623 1622	27.0 23.9
300	1.01302 1.01483	1542.47 1538.36	1.0903 1.1027	0.255 −0.293	1613 1611	28.6 25.3
1337	1.06874 1.08112	1422.80 1398.07	1.4207 1.4818	1.082 −1.210	1555 1545	35.8 32.7

energy of a nanocrystal exceeds the one of a macrocrystal (i. e., $\sigma(N) > \sigma(\infty)$). As was demonstrated in [24,26–28], this effect is attributable to the compression of a nanocrystal by surface pressure at low temperatures. It is evident from Figures 2, A and B that the decrease of function $\sigma(N)$ at $P = 0$ with a reduction in N becomes more pronounced as the temperature increases and as the nanocrystal shape deviates further from the energetically optimum one (cubic for the RP model). At $P < 20$ GPa, σ increases under isothermal compression both for a macrocrystal and a nanocrystal consisting of 306 atoms.

The lower plots in Figure 2 show baric (C) and temperature (D) dependences of the derivative of specific surface energy with respect to pressure: $\sigma'(P) = (\partial\sigma/\partial P)_T$,

10^{-3} J/(m^{2}GPa). Solid and dashed curves correspond to the results of calculation for a macrocrystal and a cubic nanocrystal. The thin solid curve in Figure 2, *C* represents the 1337 K isotherm for a rod-shaped nanocrystal. It can be seen from Figures 2, *C* and *D* that the isothermal $\sigma'(P)_T$ dependences for macro- and nanocrystals intersect at a certain pressure (P_σ): $\sigma'(P_\sigma)_{T,\infty} - \sigma'(P_\sigma)_{T,N} = 0$. The size dependence of function $\sigma'(P)_T$ changes at these points. At $P < P_\sigma$, function $\sigma'(P)_T$ increases with a reduction in N; at $P > P_\sigma$, $\sigma'(P)_T$ decreases with an isothermal-isobaric reduction in N.

It can be seen from Figures 2, *C* and *D* that $\sigma'(P)_T$ increases with an isomeric-isobaric rise of temperature. Notably, the temperature growth of function $\sigma'(P)_T$ slows down as the pressure increases.

The properties of FCC Au calculated at three different temperatures are presented in the table. The results for a macrocrystal and a cubic nanocrystal consisting of 306 atoms are listed in the first and the second rows, respectively, in each cell. The second, the third, and the fourth columns contain the values of normalized volume $v/v_o = (c/r_o)^3$, the specific surface energy of face (100), and function $\Delta_p(N) = 1 - (P_{sf}/P_{Lp})$ both for a macrocrystal at $P_{Macro} = 0$ and for a cubic nanocrystal consisting of 306 atoms at $P_{Nano} = 0$. The values of pressure P_{Nano} for a nanocrystal at $P_{Macro} = 0$ (upper row) and pressure P_{Macro} for a macrocrystal at $P_{Nano} = 0$ (lower row) are given in the fifth column (see Figure 1, *A*). The rightmost two columns present the coordinates of the maximum of function $\sigma(P)$ in Figure 2, *A*; the results for a macrocrystal and a cubic nanocrystal consisting of 306 atoms are listed in the first and the second rows, respectively, in each cell.

The expressions for isochoric and isobaric derivatives of function $\sigma(N, f)$ with respect to temperature may be derived from (2). These expressions are as follows [22–24]:

$$\sigma'(T)_v = \left(\frac{\partial\sigma}{\partial T}\right)_{c,N,f} = -\frac{3k_B R^2\gamma(N,f)}{2\alpha^{2/3}(b+2)r_o^2 k_n^*} F_E\left(\frac{\Theta_E}{T}\right), \tag{9}$$

$$\sigma'(T)_P = \left(\frac{\partial\sigma}{\partial T}\right)_{P,N,f} = \sigma'(T)_v + v\cdot\alpha_P\left(\frac{\partial\sigma}{\partial v}\right)_{T,N,f}$$

$$= \sigma'(T)_v - \frac{2}{3}\sigma\cdot\alpha_P\cdot\Delta_p. \tag{10}$$

Here, $\alpha_P = (\partial \ln v/\partial T)_P$ is the isobaric thermal volume expansion coefficient that depends on the size and the shape of a nanocrystal

$$\alpha_P = \frac{\gamma\cdot C_v}{V\cdot B_T} = \frac{3\gamma\cdot k_B\cdot F_E(\frac{\Theta_E}{T})}{B_T[\pi r_o^3/(6k_p)]}R^3,$$

where C_v is the isobaric heat capacity, B_T is the isothermal elastic modulus, and

$$F_E(y) = \frac{\partial E_w(y)}{\partial(1/y)} = \frac{y^2\exp(y)}{[\exp(y)-1]^2}.$$

Figure 3 illustrates the behavior of isochoric and isobaric derivatives of function $\sigma(100)$ with respect to temperature (in 10^{-6} J/(m$^2\cdot$K)). The upper (*A* and *B*) and lower (*C* and *D*) plots correspond to functions $\sigma'(T)_v = (\partial\sigma/\partial T)_v$ and $\sigma'(T)_P = (\partial\sigma/\partial T)_P$, respectively. Calculations were performed in accordance with formulae (9) and (10) along three isotherms (from top to bottom, for *A* and *C*: 100, 300, and 1337 K) and along three isobars (from bottom to top, for *D*: 0, 24, and 60 GPa). Solid and dashed curves correspond to the results of calculation for a macrocrystal and a cubic nanocrystal consisting of 306 atoms. Thin solid curves in Figures 3, *A* and *C* represent the 1337 K isotherm for a rod-shaped nanocrystal with 306 atoms. The results of our calculations of $\sigma'(T)_P$ for a macrocrystal of FCC Au at $P = 0$ were compared with the estimates obtained in other studies in [23,30].

It can be seen from Figure 3 that functions $\sigma'(T)_v$ and $\sigma'(T)_P$ under any pressure reach their maximum at $T = 0$ K: $\sigma'(0)_v = \sigma'(0)_P = 0$. It is evident that the values of $|\sigma'(T)_v|$ and $|\sigma'(T)_P|$ increase under arbitrary $P-T$ conditions with an isothermal-isobaric reduction in the size of a nanocrystal. The size variation of these functions becomes more pronounced as the temperature rises and as the nanocrystal shape deviates further from the energetically optimum one (cubic for the RP model). Inequality $|\sigma'(T)_v| < |\sigma'(T)_P|$ is satisfied under low pressures. However, this inequality is reversed under high pressures. Therefore, one should not equate functions $\sigma'(T)_v$ and $\sigma'(T)_P$ (as is done in certain papers). At $T \gg \Theta$, function $\sigma'(T)_v$ is almost independent of temperature and the $|\sigma'(T)_P|$ value increases with temperature. In a nanocrystal, the value of $|\sigma'(T)_i|$ increases under arbitrary $P-T$ conditions (here, $i = v$ or P).

As was noted in our study [41], function σ at $T = 0$ K should satisfy the following conditions to adhere to the third law of thermodynamics:

$$\lim_{T\to 0\,K}\left(\frac{\partial\sigma}{\partial T}\right)_{i,N} = -0,\ \lim_{T\to 0\,K}\left[\frac{\partial(\partial\sigma/\partial T)_{v,N}}{\partial v}\right]_{T,N} = -0,$$

$$\lim_{T\to 0\,K} T\left[\frac{\partial}{\partial T}\left(\frac{\partial\sigma}{\partial T}\right)_{v,N}\right]_{i,N} = -0. \tag{11}$$

Conditions (11) are valid for any crystal structure, at any given volume and pressure, and for any size and shape of a nanocrystal.

Different methods for calculation of the derivative of σ with respect to temperature in a macrocrystal have been proposed in literature. However, since the equation of state with the surface factored in was not given in these studies, it remains unclear whether the proposed expression for $\sigma'(T)$ is an isochoric derivative or an isobaric one. At the same time, it can be seen from Figure 3 that the difference between functions $\sigma'(T)_v$ and $\sigma'(T)_P$ significant and is especially pronounced at $P = 0$.

A linear approximation of the following form was used in certain studies for the isobaric or isochoric temperature dependence of the specific surface energy [42]:

$$\sigma(T) = \sigma(T = 0\,K) - \text{const}\,T. \tag{12}$$

However, it follows from Figure 3 that approximation (12) is valid only at high temperatures $T \gg \Theta$ (for $i = v$)

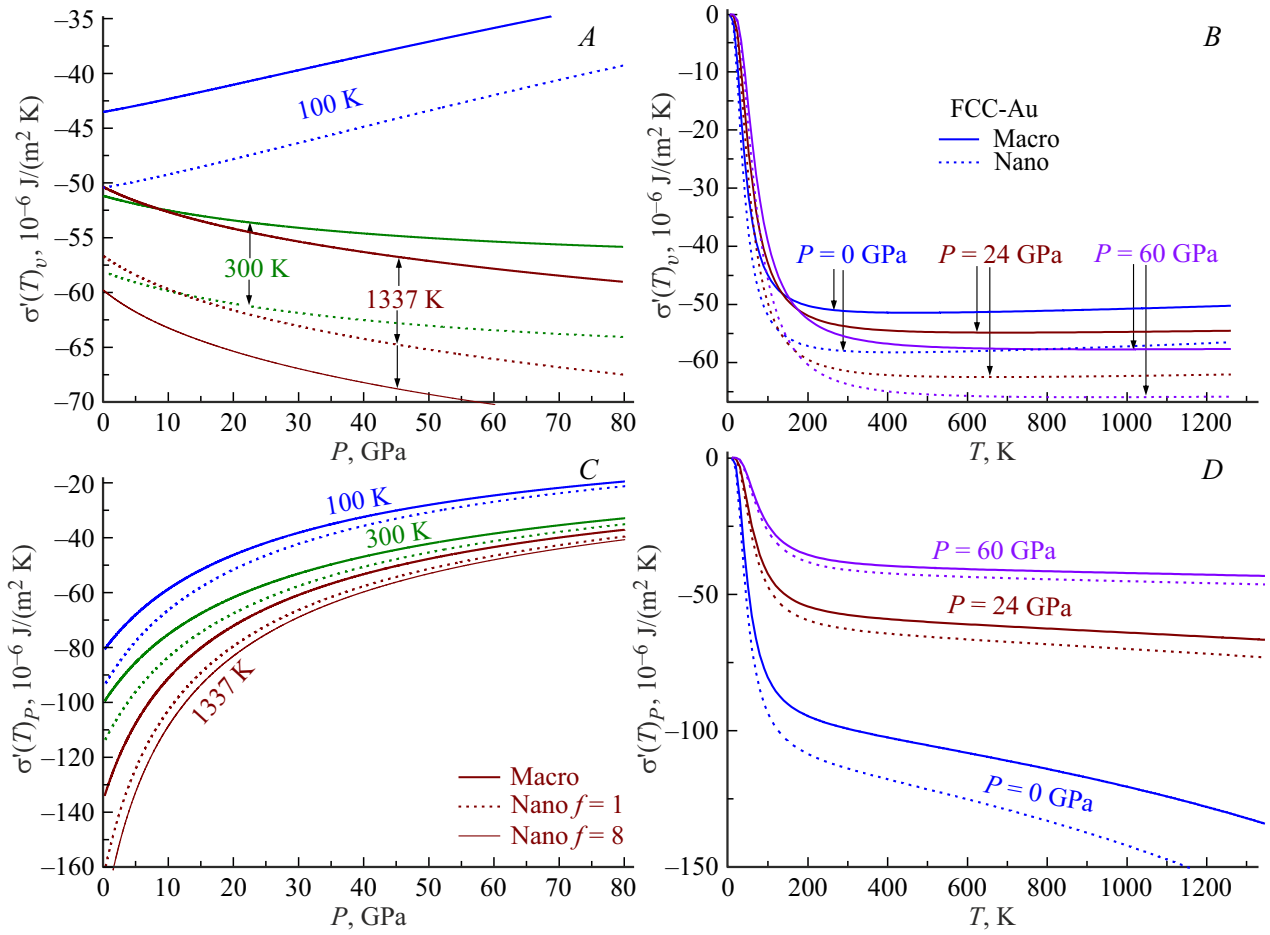

Figure 3. Behavior of isochoric (upper plots) and isobaric (lower plots) derivatives of the specific surface energy with respect to temperature for FCC Au. Isotherms of the baric dependence are shown on the left, and isobars of the temperature dependence are presented on the right. Solid and dashed curves correspond to the results of calculation for a macrocrystal and a cubic nanocrystal. Thin solid curves in Figures 3, *A* and *C* represent the 1337 K isotherm for a rod-shaped nanocrystal.

or high pressures (for $i = v$ or $i = P$). The use of approximation (12) at low temperatures can lead both to numerical errors and to violation of the third law of thermodynamics (11).

Under ultimate compression ($v/v_o \to 0$), the following relations are derived from (2)–(6) and (9) [43–45]:

$$\left.\begin{aligned}
&\lim_{v/v_o\to 0}\sigma = -\left[\frac{k_n(\infty)Da}{12\alpha^{2/3}r_o^2(b-a)}\right]\lim_{R\to\infty}R^{b+2} = -\infty,\\
&\lim_{v/v_o\to 0}\Delta_p(N,f) = 1+\lim_{R\to\infty}\frac{ab(R^b-R^a)}{2(aR^b-bR^a)} = 1+\frac{b}{2},\\
&\lim_{v/v_o\to 0}P_{sf} = \left[\frac{k_n(\infty)Dab}{6\alpha r_o^3(b-a)}\right](1-k_n^*)\lim_{R\to\infty}R^{b+3} = +\infty,\\
&\lim_{v/v_o\to 0}\sigma'(T)_v = -\frac{16Dk_n(\infty)}{45\alpha^{2/3}r_o^2[k_n^*(N,f)]^2}F_E\left(\frac{\Theta_E\max}{T}\right)\\
&\times\frac{(b-a)}{K_R ab(b+1)}\lim_{R\to\infty}R^{-b} = \max\left(\frac{\partial\sigma}{\partial T}\right)_v = -0,
\end{aligned}\right\} \quad (13)$$

where $K_R = \hbar^2/(k_B r_o^2 m)$, m is the mass of an atom, and $\hbar$ is the Planck constant.

Under ultimate tension ($v/v_o \to \infty$), (2)–(6) and (9) yield

$$\left.\begin{aligned}
&\lim_{v/v_o\to\infty}\sigma = -\left[\frac{k_BT}{4\alpha^{2/3}r_o^2k_n^*(N,f)}\right]\lim_{R\to 0}R^2 = -0,\\
&\lim_{v/v_o\to\infty}\Delta_p(N,f) = 1-\frac{abDk_n(N,f)}{6(b-a)k_BT}\lim_{R\to 0}R^a = 1,\\
&\lim_{v/v_o\to\infty}P_{sf} = -\left[\frac{k_n(\infty)Dab}{6\alpha r_o^3(b-a)}\right]\\
&\qquad\times[1-k_n^*(N,f)]\lim_{R\to 0}R^{a+3} = -0,\\
&\lim_{v/v_o\to\infty}\left(\frac{\partial\sigma}{\partial T}\right)_v = -\left[\frac{k_B}{4\alpha^{2/3}r_o^2k_n^*(N,f)}\right]\lim_{R\to 0}R^2\\
&\qquad = \max\left(\frac{\partial\sigma}{\partial T}\right)_v = -0.
\end{aligned}\right\} \quad (14)$$

Thus, it follows from (13) and (14) that the surface energy of a crystal becomes negative if it is compressed below a certain level (at $v/v_o \le (v/v_o)_{frS} < 1$) or undergoes uniform volumetric stretching to $v/v_o \ge (v/v_o)_{frL} > 1$. This is illustrated in Figure 2, *A* and has already been demonstrated in our studies [20,21,43,44]. Note that function Δ_p has a discontinuity of the second kind at fragmentation points (i.e., at $(v/v_o)_{frS}$ and $(v/v_o)_{frL}$). However, it follows from (3) that P_{sf} varies continuously.

Calculations revealed that the extent of uniform stretching under which the specific surface energy becomes negative ($(v/v_o)_{frL}$) lies in the liquid-phase region for all the examined materials (crystals of inert gases, iron, diamond, silicon, and germanium) [45]. Therefore, a crystal under uniform stretching enters a liquid phase before reaching a negative surface energy value. However, the fragmentation condition may be attained under uniaxial tension beyond the yield point.

The energy associated with surface formation is released in transition from the single-crystal state, which is unstable at $v/v_o \le (v/v_o)_{frS}$, to the energetically advantageous (by virtue of inequality $\sigma < 0$) nanostructured state. Notably, this energy increases with a reduction in the domain size achieved as a result of fragmentation of a single crystal (see [43–45]). It is also worth noting that intercrystalline surface energy of a domain σ_d in a nanostructured solid is related to the surface energy of a nanocrystal with a free surface in the following way [46]: $\sigma_d = \chi\sigma(100)$, where coefficient χ depends on the indices of contacting domain planes: $1 > \chi > 0$.

4. Discussion

Why was then an increase of σ with an isomorphic-isothermal reduction in the nanoparticle size reported in a number of studies? Let us clarify this with reference to the obtained results and using studies [5,6] as examples.

A „combination of atomistic modelling and continuum mechanics“ was used in [5] to examine a spherical core–shell model for a gold nanocrystal at $T = 0\,\mathrm{K}$. The surface pressure was characterized according to the Laplace formula, which is valid for the liquid phase, only in the surface shell layer. Compared to the bulk of the crystal, this layer was thus compressed strongly. It was then found in [5] that both the surface energy and the Young's modulus increase as the nanocrystal size decreases. This conclusion contradicts dependence $P(v/v_o)$ for macro- and nanocrystals in Figure 1 and the results reported in [36–40], where elastic modulus B_T was found to decrease with a reduction in the size of a nanocrystal. The authors of [5] have also made an error in separating an equilibrium system into two different phases (core and shell) and applying different laws to them. This violates the thermodynamic equilibrium conditions and results in strong gradients of properties over the nanocrystal volume. Equilibrium and reversible thermodynamics formulae are inapplicable to such a system.

The following formula [6, Eq. (4)] was used to calculate the specific surface energy in the computer modeling method utilized in [6] (and other theoretical studies where an increase of σ with an isomorphic-isothermal reduction in the nanoparticle size was reported):

$$\sigma(N) = \frac{E_{NP}(N) - E_{ref}(\infty)}{\Sigma},$$

where $E_{NP}(N)$ is the internal energy of a nanoparticle consisting of N atoms and $E_{ref}(\infty)$ is the internal energy of a macrocrystal.

However, a contradiction arises when functions $E_{NP}(N)$ and $E_{ref}(\infty)$ are calculated using this method: $E_{ref}(\infty)$ is calculated for a macrocrystal at $P_{Macro} = 0$, while function $E_{NP}(N)$ is calculated for a nanocrystal at $P_{Nano} > 0$. This is illustrated by Figure 1 and the table. To obtain $P_{Nano} = 0$, one needs to stretch a nanocrystal (i.e., make the specific volume or the average distance between centers of nearest-neighbor atoms in a nanocrystal greater than in a macrocrystal). This has been demonstrated experimentally in [36] for nanodiamond and in [47] for a nanocrystal of FCC ruthenium (FCC Ru). This also follows from the fact that the elastic modulus for a nanocrystal is smaller than the one for a macrocrystal at the same temperature.

Thus, a nanocrystal was compressed by surface pressure, which increased with an isomorphic-isothermal reduction in N, in those calculations where an increase of function $\sigma(N)$ with a decrease of N was reported. This compression induced an increase of function $\sigma(N)$ upon an isomorphic-isothermal reduction in the nanocrystal size.

The surface pressure for the liquid phase is much higher than the one for the solid phase at low temperatures. This is the reason why a clearly erroneous result was obtained in [6]: $\sigma_l(T = 1500\,\mathrm{K}) > \sigma_s(T = 5\,\mathrm{K})$ for both macro- and nanosystems. In the liquid phase, this result contradicts the data from [48,49], where more adequate methods were used to calculate the dimensional dependence of σ_l.

Unfortunately, the equation of state of a nanosystem has not been examined in theoretical studies where σ was found to increase with a reduction in size. This is the reason why the authors of these studies failed to notice that an isomorphic-isothermal size reduction led to a reduction in the specific volume of a nanoparticle and, as a consequence of this compression, to an increase in the specific surface energy.

5. Conclusion

Dependences of specific surface energy σ and surface pressure P_{sf} on the size and shape of a nanocrystal with a free Gibbs surface were examined under different $P-T$ conditions within equilibrium and reversible thermodynamics based on the RP model and the Mie–Lennard-Jones pair interatomic interaction potential.

The results of calculations for a macrocrystal and an FCC Au nanocrystal consisting of 306 atoms revealed

that function $P_{sf}(N)$ lies in the negative region at $P = 0$ and that $|P_{sf}(N, P = 0)|$ increases as the temperature rises and as the nanocrystal shape deviates further from the energetically optimum one (cubic for the RP model). When N decreases at $P = 0$, the decrease of function $\sigma(N)$ becomes more pronounced as the temperature increases and as the nanocrystal shape deviates further from the energetically optimum one.

These results were used to demonstrate that the conclusions made in certain studies, where an increase of function $\sigma(N)$ with an isomorphic-isothermal nanocrystal size reduction at $P = 0$ was reported, contradict the physical properties of actual metallic nanoparticles. A nanoparticle in such calculations was compressed by the surface pressure, which increased with a reduction in N. This compression led to a corresponding increase of function $\sigma(N)$ with both an isomorphic-isothermal size reduction and an isomeric (i. e., at $N = \text{const}$) nanoparticle temperature rise.

Acknowledgments

The author would like to thank S.P. Kramynin, K.N. Magomedov, Z.M. Surkhaeva, and N.Sh. Gazanova for fruitful discussions and assistance in his work.

Conflict of interest

The author declares that he has no conflict of interest.

References

[1] W.R. Tyson, W.A. Miller. Surf. Sci. **62**, *1*, 267 (1977). https://doi.org/10.1016/0039-6028(77)90442-3
[2] S.N. Zhevnenko, I.S. Petrov, D. Scheiber, V.I. Razumovskiy. Acta Materialia **205**, 116565 (2021). https://doi.org/10.1016/j.actamat.2020.116565
[3] D. Vollath, F.D. Fischer, D. Holec. Beilstein J. Nanotechnol. **9**, *1*, 2265 (2018). https://doi.org/10.3762/bjnano.9.211
[4] X. Zhang, W. Li, H. Kou, J. Shao, Y. Deng, X. Zhang, J. Ma, Y. Li, X. Zhang. J. Appl. Phys. **125**, *18*, 185105 (2019). https://doi.org/10.1063/1.5090301
[5] D. Holec, L. Löfler, G.A. Zickler, D. Vollath, F.D. Fischer. Int. J. Solids. Structures **224**, 111044 (2021). https://doi.org/10.1016/j.ijsolstr.2021.111044
[6] H. Amara, J. Nelayah, J. Creuze, A. Chmielewski, D. Alloyeau, C. Ricolleau, B. Legrand. Phys. Rev. B **105**, *16*, 165403 (2022). https://doi.org/10.1103/PhysRevB.105.165403
[7] E.H. Abdul-Hafidh. J. Nanoparticle Res. **24**, *12*, 266 (2022). https://doi.org/10.1007/s11051-022-05638-6
[8] R.C. Tolman. J. Chem. Phys. **17**, *3*, 333 (1949). https://doi.org/10.1063/1.1747247
[9] K.K. Nanda. Phys. Lett. A **376**, *19*, 1647 (2012). https://doi.org/10.1016/j.physleta.2012.03.055
[10] H.M. Lu, Q. Jiang. Langmuir **21**, *2*, 779 (2005). https://doi.org/10.1021/la0489817
[11] S. Xiong, W. Qi, Y. Cheng, B. Huang, M. Wang, Y. Li. Phys. Chem. Chem. Phys. **13**, *22*, 10648 (2011). https://doi.org/10.1039/C0CP02102D
[12] S. Ono, S. Kondo. Molecular Theory of Surface Tension in Liquids. In: Structure of Liquids. Springer, Berlin, Heidelberg (1960). P. 134–280. https://doi.org/10.1007/978-3-642-45947-4_2
[13] S.S. Rekhviashvili. Colloid J. **82**, *3*, 342 (2020). https://doi.org/10.1134/S1061933X20030084
[14] J. Wang, S.Q. Wang. Surf. Sci. **630**, 216 (2014). https://doi.org/10.1016/j.susc.2014.08.017
[15] S. De Waele, K. Lejaeghere, M. Sluydts, S. Cottenier. Phys. Rev. B **94**, *23*, 235418 (2016). https://doi.org/10.1103/PhysRevB.94.235418
[16] M.N. Magomedov. Tech. Phys. **59**, *5*, 675 (2014). https://doi.org/10.1134/S1063784214050211
[17] V.D. Nguyen, F.C. Schoemaker, E.M. Blokhuis, P. Schall. Phys. Rev. Lett. **121**, *24*, 246102 (2018). https://doi.org/10.1103/PhysRevLett.121.246102
[18] D. Kim, J. Kim, J. Hwang, D. Shin, S. An, W. Jhe. Nanoscale **13**, *14*, 6991 (2021). https://doi.org/10.1039/d0nr08787d
[19] M.X. Lim, B. VanSaders, A. Souslov, H.M. Jaeger. Phys. Rev. X **12**, *2*, 021017 (2022). https://doi.org/10.1103/PhysRevX.12.021017
[20] M.N. Magomedov. Phys. Solid State **46**, *5*, 954 (2004). https://doi.org/10.1134/1.1744976
[21] M.N. Magomedov. Crystallogr. Reps **62**, *3*, 480 (2017). https://doi.org/10.1134/S1063774517030142
[22] M.N. Magomedov. J. Surf. Investigation. X-ray, Synchrotron. Neutron Techniques **14**, *6*, 1208 (2020). https://doi.org/10.1134/S1027451020060105
[23] M.N. Magomedov. Phys. Solid State **63**, *10*, 1465 (2021). https://doi.org/10.1134/S1063783421090250
[24] M.N. Magomedov. Phys. Solid State **62**, *12*, 2280 (2020). https://doi.org/10.1134/S1063783420120197
[25] E.N. Ahmedov. Physica B: Condens. Matter **571**, 252 (2019). https://doi.org/10.1016/j.physb.2019.07.027
[26] S.P. Kramynin. J. Phys. Chem. Solids **152**, 109964 (2021). https://doi.org/10.1016/j.jpcs.2021.109964
[27] S.P. Kramynin. Phys. Met. Metallography **123**, *2*, 107 (2022). https://doi.org/10.1134/S0031918X22020065
[28] S.P. Kramynin. Solid State Sci. **124**, 106814 (2022). https://doi.org/10.1016/j.solidstatesciences.2022.106814
[29] R. Briggs, F. Coppari, M.G. Gorman, R.F. Smith, S.J. Tracy, A.L. Coleman, A. Fernandez-Pañella, M. Millot, J.H. Eggert, D.E. Fratanduono. Phys. Rev. Lett. **123**, *4*, 045701 (2019). https://doi.org/10.1103/PhysRevLett.123.045701
[30] M.N. Magomedov. Phys. Solid State **64**, *7*, 765 (2022). https://doi.org/10.21883/PSS.2022.07.54579.319
[31] M.N. Magomedov. Phys. Solid State **65**, *5*, 708 (2023). https://doi.org/10.21883/PSS.2023.05.56040.46
[32] F. Ercolessi, W. Andreoni, E. Tosatti. Phys. Rev. Lett. **66**, *7*, 911 (1991). https://doi.org/10.1103/physrevlett.66.911
[33] S.L. Lai, J.Y. Guo, V. Petrova, G. Ramanath, L.H. Allen. Phys. Rev. Lett. **77**, *1*, 99 (1996). https://doi.org/10.1103/PhysRevLett.77.99
[34] Y. Qi, T. Çağin, W.L. Johnson, W.A. Goddard III. J. Chem. Phys. **115**, *1*, 385 (2001). https://doi.org/10.1063/1.1373664
[35] G. Kellermann, A.F. Craievich. Phys. Rev. B **78**, *5*, 054106 (2008). https://doi.org/10.1103/physrevb.78.054106
[36] M. Mohr, A. Caron, P. Herbeck-Engel, R. Bennewitz, P. Gluche, K. Brühne, H.-J. Fecht. J. Appl. Phys. **116**, *12*, 124308 (2014). https://doi.org/10.1063/1.4896729

[37] A. Rida, E. Rouhaud, A. Makke, M. Micoulaut, B. Mantisi. Philosoph. Mag. **97**, *27*, 2387 (2017). https://doi.org/10.1080/14786435.2017.1334136
[38] M. Goyal, B.R.K. Gupta. Modern Phys. Lett. B **33**, *26*, 1950310 (2019). https://doi.org/10.1142/s021798491950310x
[39] J. Li, B. Lu, H. Zhou, C. Tian, Y. Xian, G. Hu, R. Xia. Phys. Lett. A **383**, *16*, 1922 (2019). https://doi.org/10.1016/j.physleta.2018.10.053
[40] I.M. Padilla Espinosa, T.D.B. Jacobs, A. Martini. Nanoscale Res. Lett. **17**, *1*, 96 (2022). https://doi.org/10.1186/s11671-022-03734-z
[41] M.N. Magomedov. J. Surf. Investigation. X-ray, Synchrotron. Neutron Techniques **6**, *1*, 86–91 (2012). https://doi.org/10.1134/S1027451012010132
[42] S. Zhu, K. Xie, Q. Lin, R. Cao, F. Qiu. Advances. Colloid. Interface Sci. **315**, 102905 (2023). https://doi.org/10.1016/j.cis.2023.102905
[43] M.N. Magomedov. J. Surf. Investigation. X-ray, Synchrotron. Neutron Technique **6**, *3*, 430 (2012). https://doi.org/10.1134/S1027451012050151
[44] M.N. Magomedov. J. Surf. Investigation. X-ray, Synchrotron. Neutron Technique **7**, *6*, 1114 (2013). https://doi.org/10.1134/S1027451013060104
[45] M.N. Magomedov. Tech. Phys. **61**, *5*, 722 (2016). https://doi.org/10.1134/S1063784216050145
[46] S.N. Zadumkin, A.A. Karashaev. In: Poverkhnostnye yavleniya v rasplavakh i voznikayushchikh iz nikh tverdykh fazakh. Kabard.-Balkar. Kn. Izd., Nal'chik (1965). pp. 85–88. (in Russian).
[47] M. Zhao, Y. Xia. Nature Rev. Mater. **5**, *6*, 440 (2020). https://doi.org/10.1038/s41578-020-0183-3
[48] S.W. Cui, J.A. Wei, Q. Li, W.W. Liu, P. Qian, X.S. Wang. Chinese Phys. B **30**, *1*, 016801 (2021). https://doi.org/10.1088/1674-1056/abb65a
[49] S. Gong, Z. Hu, L. Dong, P. Cheng. Phys. Fluids **35**, *7*, 073315 (2023). https://doi.org/10.1063/5.0155289

Translated by D.Safin